Journal Pre-proof

On-machine workpiece straightness profile measurement using a hybrid Fourier 3-sensor method

Pu Huang, Shengyu Shi, Jin Xie, Han Haitjema, Zengyuan Niu, Quanpeng He, Kuo Lu

PII: S0141-6359(22)00219-7

DOI: https://doi.org/10.1016/j.precisioneng.2022.10.002

Reference: PRE 7618

To appear in: *Precision Engineering*

Received Date: 9 March 2022

Revised Date: 12 July 2022

Accepted Date: 8 October 2022

On-machine workpiece straightness profile measurement using a hybrid Fourier 3-sensor method

Authors: Pu Huang[1], Shengyu Shi[*, 1], Jin Xie[*, 1], Han Haitjema[2], Zengyuan Niu[3], Quanpeng He[1], Kuo Lu[1]

1. School of Mechanical and Automobile Engineering, South China University of Technology, Guangzhou, 510640, P.R. China

2. Manufacturing Metrology Section, Manufacturing, Processes and Systems (MaPS), Department of Mechanical Engineering, KU Leuven, 3001 Leuven, Belgium

3. Jiangsu JITRI High Value Manufacturing Co. Ltd., Kunshan, 215335, P.R. China

Email addresses: shisy@scut.edu.cn (S. Shi); jinxie@scut.edu.cn (Jin Xie)

Declarations of interest

None

[*] Corresponding author. Tel.: 0086 (020) 87114578; Fax: 0086 (020) 87112503

Abstract

To compensate for the straightness error of the slide of a machine tool efficiently and precisely, on-machine self-calibrating measurement of the manufacturing error is critical. The Fourier 3-sensor (F3S) method proposed by Fung is promising in measuring the straightness profile of a workpiece accurately on a machine. However, it still suffers from two main challenges: the height difference between the second and the third probes and the stochastic uncertainty, both of which can significantly decrease the measurement precision. In this paper, we counter these two challenges, respectively, and propose the solutions accordingly. First of all, by resorting to the Laplace transform, an algorithm for the F3S method is proposed. Second, the adverse effect of the height difference between the second and the third probes is demonstrated. An approach is presented for estimating the height difference, and compensating for this. Third, to alleviate the stochastic uncertainty, a hybrid F3S method is developed: several F3S measurements are first performed under different probe spacings; then, the optimal Fourier coefficients of the straightness profile are individually selected from the candidate estimates in accordance to the determinant of the transfer matrix. Finally, practical straightness profile measurements were performed, respectively, on a grinding machine by adopting the hybrid F3S method and on a Taylor Hobson surface profiler. The results show that compared with the conventional F3S method, the hybrid F3S method reduced the measurement uncertainty significantly, and the straightness profiles estimated by the hybrid method and by the surface profiler were consistent with each other.

Keywords: Straightness measurement, On-machine self-calibrating measurement, Hybrid Fourier 3-sensor method, Height difference, Measurement uncertainty

1. Introduction

Almost perfect flat/straight surfaces are required for various components, such as silicon wafers [1], optical mirrors [2], guideways [3, 4], etc., as the straightness determines the performance of the components, as well as the systems in which these are used. To fabricate the workpieces satisfying the tight flatness/straightness tolerance, ultra-precision machining tools are fundamental. However, as the demand for higher performance of the product grows continuously, the readily achievable accuracy is limited relatively, especially due to the error motion of rotary/slide axes of the machine tools, which will be mapped onto the surface topography of the manufactured parts [5], as demonstrated in Fig. 1.

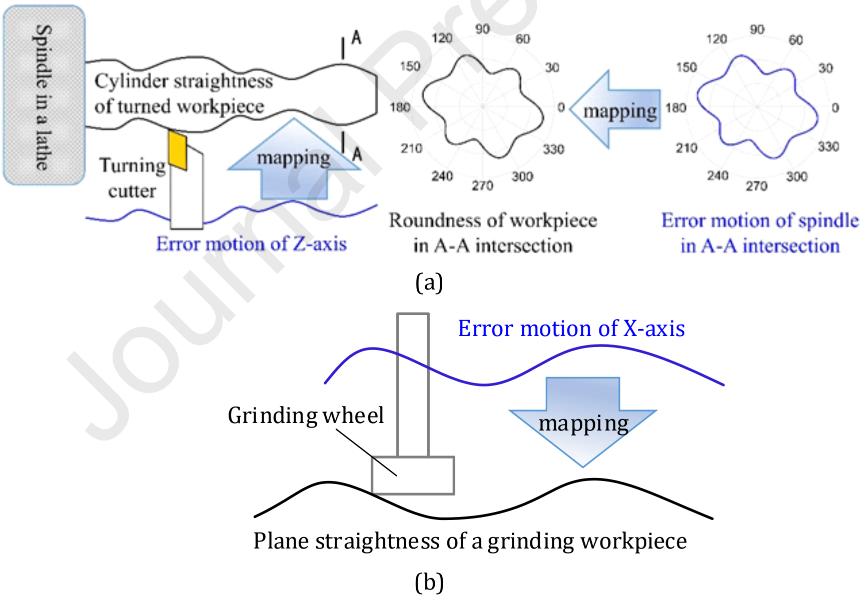

Fig. 1. Error motion of tools, (a) in a turning process, the error motion of the Z-axis in the X direction determines the cylinder straightness of the machined parts and (b) in a grinding process, the straightness error motion of the linear axis will be mapped onto the manufactured surface.

Error compensation machining, during which the machining deviation of the workpiece from the designed nominal shape will be evaluated and then fed back to the NC controller, is considered a universally applicable and cost-effective approach in diminishing the machining error [6-9].

For compensation machining, precise measurement of surface machining error is imperative and critical. The strategies for measuring the surface form error can generally be categorized into two groups: (a) on-machine measurements that are carried out on the machining tools where the workpieces are manufactured and (b) off-machine measurements that are made by a stand-alone profilometer [8]. Compared with the off-machine measurements, the on-machine measurements can be performed soon after the manufacturing process (or even while the machining process is taking place), without the requirement to move the workpiece from the machining tool to the measuring instrument. Accordingly, the compensation machining can also be conducted immediately afterward the inspection, without the need to return the workpiece to the machining tools from the measuring instruments. Adoption of the on-machine measurement can shorten the whole process flow of compensation machining: repeated assembly and disassembly processes, along with tedious calibration of the initial position of the workpiece after its movements, are avoided. Thus, the efficiency is raised significantly. Meanwhile, the accuracy of both the measurement and the compensation could also be enhanced.

However, during the on-machine measurement, the straightness/roundness error of the manufactured workpiece is at the same level as the error motions of slide/rotary axes of the machine tools, which will be superposed into the measurement result and are major sources of the measurement error [8]. Therefore, the error motion of the machine tool axes cannot be ignored and error separation techniques, also termed self-calibrating techniques, should be employed to reduce their adverse effect.

This paper will investigate the ultra-precision on-machine measurement of straightness profiles, especially focusing on self-calibrating measurement techniques.

The concept of the self-calibrating straightness measurement was originally proposed by Whitehouse in 1978 [10]. Since then, this technique has been intensively studied from different perspectives, considering for example, the measuring setup (implementation), the algorithm, and the measurement uncertainty. In the early 1980s, Tozawa et al. [11, 12] presented the sequential-two-points (S-2P) method, where two distance sensors are attached on and move together with the slide table to measure the interval variation between the slide guideway and the workpiece surface. Then, the slide error motion could be canceled by computing the difference between the two sensor outputs. Finally, the profile of the workpiece could be recovered by an iterative accumulation of the differential output. A remarkable advantage of the S-2P method is that the straightness of both the slide and the workpiece can be estimated simultaneously. However, at least three problems were also observed associated with the S-2P method:

(1) Apart from straightness error motion, the slide also has yaw/pitching error motion, which contributes to the probe reading as well. To separate both types of error motion, Elster proposed the traceable multi-sensor (TMS) method, where an additional autocollimator was adopted to directly detect the angular error motion [13]; in 1986, Tanaka [14] extended the S-2P to present the sequential-three-points method (S-3P), which can separate the influences from not only the straightness error motion but also the yaw error motion of the slide.

(2) In Ref. [14], Tanaka proved that a height difference of the two sensors (zero-difference) in the sensing direction makes a linear increment term in the measurement result. This difference could be reduced either by manually aligning the two sensors or post-processing the collected

signals [14]. In Ref. [15], Gao proved that in the S-3P, the height differences between the three probes would also introduce a parabolic error term in the profile evaluation result. To solve this issue, he presented a scanning multi-probe system, where 6 probes are employed [15]. This problem was also solved by Dr. Elster, where an additional autocollimator was adopted [16].

(3) Besides, in the original S-2P/S-3P straightness measurements, the sampling interval equals the separation distance between the two sensors, which implies that the sampled data points can be too sparse to characterize the workpiece profile accurately, especially for the high-order undulations. To overcome this limit, Kiyono and Gao put forward the generalized 2-point method (G-2P) [17, 18] and the generalized 3-point method (G-3P) [19] where the sampling interval is much smaller than the spacing between the two sensors, and accordingly, the algorithm to estimate the workpiece profile is replaced by integration of the differential output of the two sensors with steps equaling the sampling interval. However, the generalized methods could only give an approximate estimation for the workpiece profile.

Besides, in 1996, Li [20] presented a different algorithm by resorting to the discrete Fourier transform to solve the sequential two-point/three-point straightness measurement. In his algorithm, the sampling interval was no longer limited to the probe spacing and can be as small as possible. This means that the tangential resolution of the estimated profile could be significantly increased. However, Li's algorithm requires that the straightness profile should recur at a regular interval of the testing length, which, unfortunately, is not always the case. Hence, when the second probe moves out of the measuring section, a non-target profile was inspected and an unexpected discrepancy could result in the estimation.

To overcome this issue, Fung [21] described a novel treatment where a third probe is utilized to rectify the second probe signal: when the second probe moves out of the measuring area, its data acquisition will be suspended and the third probe, which is separated with a distance of the measuring length from the second probe, will continue the data reading to supplement/rectify the second signal. Consequently, the joint signal becomes a summation of the slide error motion and the targeted workpiece profile. This revised two-probe method, also named the Fourier 3-sensor (F3S) method [21] is later extended to the Fourier 5-sensor (F5S) method after considering the yaw error motion of the slide [22, 23].

After employing the Fourier-based algorithm, it is no longer required that the tips of the first and the second probes should be at the same height. But it is required that the tips of the second and the third probes should be at the same height. Otherwise, the joint signal will be erroneous and the estimation result will be incorrect. One of the targets of this paper is to unveil the effect of the height difference of the probes on the measurement result. Based on this, a solution will be proposed.

In theory, the profile of the workpiece can be perfectly estimated without systematic calculating error after adopting Fung's measuring setup and the Fourier-based algorithm, which practically had also been successfully used for roundness measurements [24]. However, like the roundness measurements [25-27], the F3S straightness measurements suffer from remarkable uncertainty as well, which may come from the stochastic probe noise and the installation deviation of the sensors. Therefore, to achieve the highest precision of straightness profile measurement, another target of this paper is to analyze the measurement uncertainty of the F3S method. Based on this, a solution will be proposed.

The rest of this paper is organized as follows. In Section 2, by resorting to the Laplace transform, an algorithm of the F3S method will be described. In Section 3, the adverse effect of the height difference between the second and the third probes will be analyzed; and then, a solution of data preprocessing will be proposed for removing this effect. In Section 4, a hybrid algorithm in the harmonic domain is described aiming at measurement precision self-calibrating. In Section 5 and 6, practical straightness measurements are carried out on a grinding machine. The conclusion is drawn in Section 7.

2. Principle of the F3S method

2.1 Laplace-transform-based algorithm of the F3S method

In the original Fourier-based 2-Sensor (F2S) method [20], two displacement sensors/probes P_1 and P_2, separated by a spacing of d, are employed and mounted on a linear moving slide to measure the workpiece profile, as shown in Fig. 2.

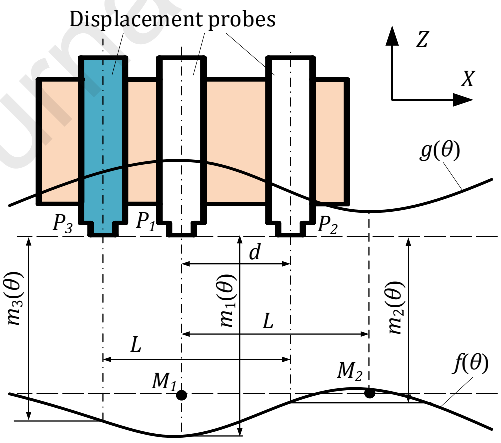

Fig. 2. Schematic diagram of Fourier 2-sensor/3-sensor method.

Thus, when the first probe P_1 moves from M_1 to M_2, the reading of the two probes, $m_1(\theta)$ and $m_2(\theta)$, can be written as:

$$m_1(\theta) = A_1 + f(\theta) + g(\theta),\ \ (0 \leq \theta < 2\pi) \tag{1}$$

$$m_2(\theta) = A_2 + f\left(\theta + \frac{2\pi d}{L}\right) + g(\theta),\ (0 \leq \theta < 2\pi) \tag{2}$$

respectively. Here, $g(\theta)$ stands for the straightness error motion of the slide; $f(\theta)$ stands for the straightness error of the workpiece profile; the region between M_1 and M_2 is the measurement section, and its length equals L. θ is the equivalent angular position of the probe P_1, calculated from $\theta = \frac{2\pi x}{L}$; x is the actual position of P_1 along the X-axis. A_1 and A_2 are the initial outputs of P_1 and P_2, which can be numerically removed as they do not affect the estimation result.

Clearly, the readings m_1 and m_2 are both the summation of the slide error motion $g(\theta)$ and the workpiece profile $f(\theta)$, which, however, contains a phase shift caused by the probe position. Then, to calculate $f(\theta)$, four steps are still required as follows:

Step 1. Calculate the difference between $m_1(\theta)$ and $m_2(\theta)$ to eliminate the slide error motion $g(\theta)$:

$$m(\theta) = m_1(\theta) - m_2(\theta) = f(\theta) - f(\theta + \frac{2\pi d}{L}) \tag{3}$$

Here, $m(\theta)$ is usually called the weighted function.

Step 2. Apply the Laplace transform to Eq. (3):

$$F(s) = \frac{1}{1 - e^{\frac{2\pi d}{L}s}} M(s) \tag{4}$$

Here, $F(s)$ and $M(s)$ are the Laplace transform of $f(\theta)$ and $m(\theta)$, respectively.

Step 3. Substitute $s = j\omega$ into Eq. (4):

$$F(j\omega) = \frac{1}{1 - e^{j\frac{2\pi d}{L}\omega}} M(j\omega) \tag{5}$$

In this way, the Fourier coefficients of the workpiece profile $F(j\omega)$ can be evaluated. Here, $M(j\omega)$ are the Fourier coefficients of $m(\theta)$, which can be computed by applying the Fourier transform to $m(\theta)$. ω is the harmonic order, which equals …, -2, -1, 0, 1, 2, …

Step 4. Apply the inverse Fourier transform to $F(j\omega)$:

$$f(\theta) = F^{-1}[F(j\omega)] \tag{6}$$

In this way, the workpiece profile $f(\theta)$ is finally estimated.

We can find that by resorting to the Laplace transform, the workpiece profile can be conveniently recovered from the superposed signals to separate the slide error motion. However, the F2S method is accurate only if the workpiece profile is periodic with a length of L [20]

$$f(\theta) = f(\theta + 2\pi), \tag{7}$$

or at least

$$f(\theta) = f(\theta + 2\pi), \quad \left(0 < \theta < \frac{2\pi d}{L}\right). \tag{8}$$

Otherwise, the Laplace transform of $f\left(\theta + \frac{2\pi d}{L}\right), (0 < \theta < 2\pi)$, contained in the second probe signal $m_2(\theta)$, is not equal to $e^{\frac{2\pi d}{L}s}F(s)$.

To solve this issue, Fung presented the F3S method [21], which employs a third probe P_3 to rectify the second probe signal. In his method, P_3 is separated from P_2 by a spacing of L, as indicated by the blue sensor in Fig. 2. And, when the second probe P_2 moves out of the measurement section, its data acquisition will be suspended and the third probe P_3 will continue the data reading to supplement the second signal. Thus, the rectified/joint signal $m_{r2}(\theta)$ can be mathematically formulated as follows:

$$m_{r2}(\theta) = \begin{cases} m_2(\theta) = A_2 + f\left(\theta + \frac{2\pi d}{L}\right) + g(\theta), \left(0 \le \theta < \frac{2\pi d}{L} - 2\pi\right) \\ m_3(\theta) = A_3 + f\left(\theta + \frac{2\pi d}{L} - 2\pi\right) + g(\theta), \left(\frac{2\pi d}{L} - 2\pi \le \theta < 2\pi\right) \end{cases} \tag{9}$$

Here, A_3 is the initial output of P_3.

In the joint signal $m_{r2}(\theta)$, the workpiece profile component can be appropriately obtained by circle-shifting the workpiece profile $f(\theta)$ by a phase of $\frac{2\pi d}{L}$. Hence, its Laplace transform is properly equal to $e^{\frac{2\pi d}{L}s}F(s)$. Theoretically, after replacing the $m_2(\theta)$ by the $m_{r2}(\theta)$ in Eq. (3-6), the workpiece profile can be accurately estimated.

2.2 Simulation of the F3S method to measure a non-periodical profile

For a demonstration of the applicability of the F3S method in measuring a non-periodical profile, a numerical simulation was carried out. Both the workpiece profile and the slide error motion contain harmonics of 1~30 order, which denotes that there are 1~30 undulations within the length L. In addition, to construct a non-periodical feature, a step (as highlighted by the yellow bar in Fig. 3), as well as a slope component is added to the workpiece profile.

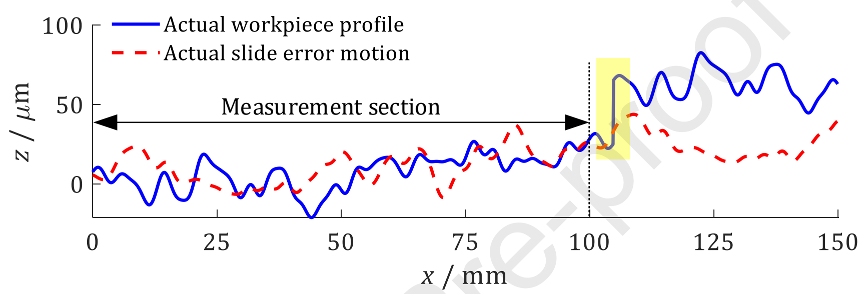

Fig. 3. Actual workpiece profile and slide error motion.

The mathematical expression of the workpiece profile and the slide error motion are detailed in Eq. (10-11):

$$\overline{f(\theta)} = \begin{cases} \sum_{\omega=1}^{N} 7e^{-0.12\omega}\cos(\omega\theta + \varphi_{\omega f}) + 0.2\theta, \left(0 \le \theta < \frac{21\pi}{10}\right) \\ \sum_{\omega=1}^{N} 7e^{-0.12\omega}\cos(\omega\theta + \varphi_{\omega f}) + 0.2\theta + 40, \left(\frac{21\pi}{10} \le \theta < 3\pi\right) \end{cases} \quad (10)$$

$$\overline{g(\theta)} = \sum_{\omega=1}^{N} 5e^{-0.08\omega}\cos(\omega\theta + \varphi_{\omega g}), \left(0 \le \theta < \frac{3\pi}{2}\right) \quad (11)$$

Here, $\overline{f(\theta)}$ and $\overline{g(\theta)}$ denote the actual workpiece profile and the actual slide error motion, respectively; $\varphi_{\omega f}$ and $\varphi_{\omega g}$ are arbitrary phases of the ω^{th} order harmonic; N, which equals 30 orders in this paper, is the cut-off order. The measurement section is from 0 to 100 mm, namely, the measurement length $L = 100$ mm. Hence, the probe signal $m_1(\theta)$, $m_2(\theta)$, $m_3(\theta)$, and the joint signal $m_{r2}(\theta)$ can be constructed.

Fig. 4 depicts the estimation results of the workpiece profiles by both the F2S and the F3S methods, where the probe spacing d was 11.40 mm; also, the trend term was removed for a clearer comparison. Clearly, the workpiece profile in both the spatial (Fig. 4a) and the harmonic domains (Fig. 4b) can almost be perfectly estimated by the F3S method while the F2S method suffers from an obvious deviation, illustrating the feasibility of the F3S method in measuring a non-periodical profile.

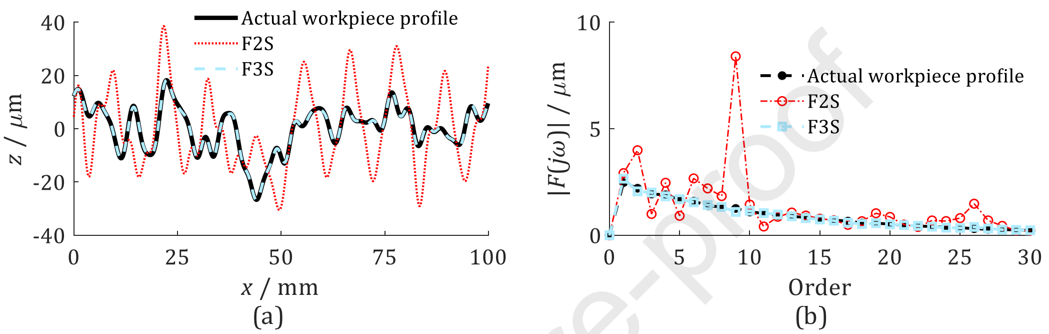

Fig. 4. Estimated results of the F3S method and the F2S method (a) in the spatial and(b) harmonic domains.

3. Effect of the height difference between probes

3.1 Effect of height difference between probes

In subsection 2.1, we employ the signal $m_3(\theta)$ to rectify the signal $m_2(\theta)$, to construct an integrated periodical signal, i.e. the joint signal $m_{r2}(\theta)$. However, in practice, there is always an installation error, i.e. a height difference α_h between the second and third probes, as illustrated in Fig. 5(a). Under this condition, if we still merge $m_3(\theta)$ and $m_2(\theta)$ directly, the constructed $m_{r2}(\theta)$ will be erroneous. Ideally (without height difference), the third probe signal should be as the green dashed line $m_3^{'}(\theta)$, but in practice, due to the height difference, the red line $m_3(\theta)$ is sampled and merged into the joint signal $m_2(\theta)$, as shown in Fig. 5 (b). Consequently, a significant error will be introduced in the measurement result.

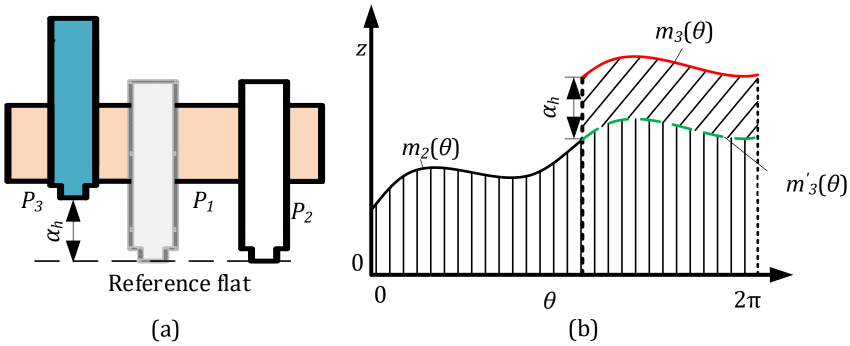

Fig. 5. The effect of height difference of the probes, (a) demonstration of the height difference, and (b) demonstration of the resulting error in the joint signal $m_{r2}(\theta)$.

3.2 Cancellation of the adverse effect of probe height difference

To ensure the accuracy of the F3S measurement, the height difference must be compensated. In general, the height difference can be reduced by adjusting the probes carefully through inspecting a reference plane. This process, however, is time-consuming, and sometimes cannot be accurate enough, as a perfect reference plane is always unachievable. Hence, in this section, we propose a numerical method to cancel the adverse influence of the height difference.

In practical measurements, there are possibly two conditions regarding the positioning of the workpiece and the guideway: parallel to each other or not.

Condition 1: the guideway and the workpiece are parallel to each other

Under this condition, $g(0) = g(2\pi) = 0$ and $f(0) = f(2\pi) = 0$. At the joint point, the readings of the second and the third probes are given by:

$$m_2\left(2\pi - \frac{2\pi d}{L}\right) = A_2 + f(2\pi) + g(2\pi - \frac{2\pi d}{L}) \tag{12}$$

$$m_3\left(2\pi - \frac{2\pi d}{L}\right) = A_3 + f(0) + g(2\pi - \frac{2\pi d}{L}) \tag{13}$$

Since $f(0) = f(2\pi) = 0$, the height difference between the second and the third probe can be given by the difference of the two probe readings at the joint point:

$$\alpha_h = A_2 - A_3 = m_2\left(2\pi - \frac{2\pi d}{L}\right) - m_3\left(2\pi - \frac{2\pi d}{L}\right) \quad (14)$$

Hence, the influence of height difference in $m_3(\theta)$ can be easily canceled by the following equation:

$$m_3'(\theta) = m_3(\theta) + \alpha_h = m_3(\theta) + m_2\left(2\pi - \frac{2\pi d}{L}\right) - m_3\left(2\pi - \frac{2\pi d}{L}\right) \quad (15)$$

Thus, a correct joint signal $m_{r2}(\theta)$ can be constructed by jointing $m_3'(\theta)$ to $m_2(\theta)$.

Condition 2: the guideway and the workpiece are not parallel to each other

In practice, the guideway and the workpiece are usually not parallel to each other. Under this condition, $g(0) = g(2\pi) = 0$ and $f(0) = 0 \neq f(2\pi) = 2\pi k$. Here, we assume that the direction of the guideway is the reference direction; k stands for the slope of the workpiece relative to the guideway, which causes a linear increment term to all the probe signals.

Under this assumption, readings of the second and the third probes at the joint point are:

$$m_2\left(2\pi - \frac{2\pi d}{L}\right) = A_2 + f(2\pi) + g\left(2\pi - \frac{2\pi d}{L}\right) = A_2 + 2\pi k + g\left(2\pi - \frac{2\pi d}{L}\right) \quad (16)$$

$$m_3\left(2\pi - \frac{2\pi d}{L}\right) = A_3 + f(0) + g(2\pi - \frac{2\pi d}{L}) \quad (17)$$

From Eq. (16-17), we can derive that the height difference between the second and the third probe is given by

$$\alpha_h = A_2 - A_3 = m_2\left(2\pi - \frac{2\pi d}{L}\right) - m_3\left(2\pi - \frac{2\pi d}{L}\right) - 2\pi k \quad (18)$$

Since $m_1(\theta) = A_1 + f(\theta) + g(\theta)$, $g(0) = g(2\pi) = 0$, and $f(0) = 0 \neq f(2\pi) = 2\pi k$, we can further prove that the $2\pi k$ can be estimated by the difference between $m_1(2\pi)$ and $m_1(0)$, as follows:

$$m_1(2\pi) - m_1(0) = [A_1 + f(2\pi) + g(2\pi)] - [A_1 + f(0) + g(0)] = f(2\pi) - f(0) = 2\pi k \quad (19)$$

Therefore, the height difference in $m_3(\theta)$ can be compensated by:

$$m_3'(\theta) = m_3(\theta) + \alpha_h = m_3(\theta) + m_2\left(2\pi - \frac{2\pi d}{L}\right) - m_3\left(2\pi - \frac{2\pi d}{L}\right) - 2\pi k = m_3(\theta) + m_2\left(2\pi - \frac{2\pi d}{L}\right) - m_3\left(2\pi - \frac{2\pi d}{L}\right) - m_1(2\pi) + m_1(0) \quad (20)$$

Please note that Eq. (20) is a general equation to compensate for the height difference in the third probe signal.

3.3 A simulation to compensate for the height difference

To verify the effectiveness of the approach in compensating for the height difference, a simulation was carried out. $\overline{f(\theta)}$ and $\overline{g(\theta)}$ defined in subsection 2.2 were still used here; d equaled 34.10 mm; the height difference between P_2 and P_3 was 50 μm.

Fig. 6(a) and 6(b) show the signals before and after the compensation, respectively. In Fig. 6(a), a step of 30 μm can be observed in the joint signal $m_{r2}(\theta)$ as highlighted by yellow bars while it was cancelled after compensation as shown in Fig. 6(b).

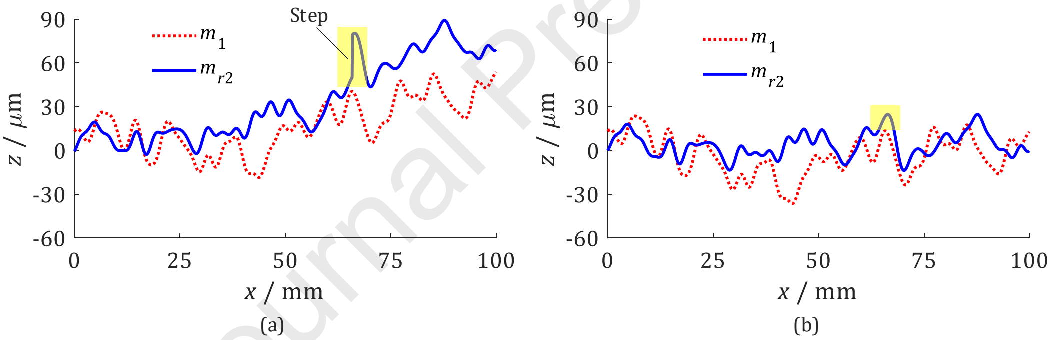

Fig. 6 Signals of $m_1(\theta)$ and $m_{r2}(\theta)$, before (a) and after (b) the compensation of the height difference.

The estimation results of the profile are shown in Fig. 7. For a clearer comparison, the trend terms in the estimated profiles and the actual ones were removed. A large discrepancy can be observed before the compensation: more than 15 μm in the spatial domain (Fig. 7 (a)) and about 4 μm in the harmonic domains (Fig. 7 (b)). But, after compensation, the discrepancy was almost completely eliminated.

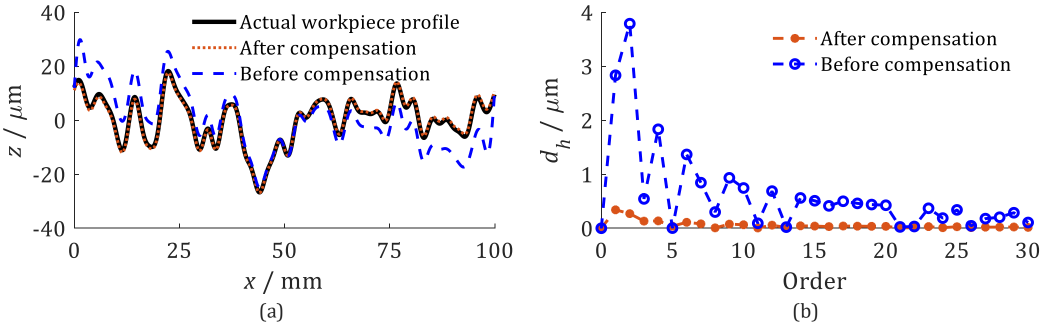

Fig. 7. The measurement results before and after compensation of the probes height difference (a) the spatial domain and (b) harmonic deviation.

To quantify the overall measurement accuracy, three criteria are defined here: the overall measurement deviation d_{sp}, the overall harmonic deviation D_h, and the harmonic deviation d_h.

$$d_{sp} = \frac{1}{N_s}\sum_{k=1}^{N_s}\left|f_{es}(k) - \overline{f(k)}\right| \quad (21)$$

Here, $f_{es}(k)$ and $\overline{f(k)}$ are the estimated workpiece profile and the actual one, respectively. N_s is the total number of sampling points.

$$D_h = \frac{1}{N}\sum_{\omega=1}^{N}\left||F_{es}(j\omega)| - |\overline{F(j\omega)}|\right| \quad (22)$$

Here, $F_{es}(j\omega)$ and $\overline{F(j\omega)}$ are the harmonic coefficients of $f_{es}(k)$ and $\overline{f(k)}$, respectively.

$$d_h(\omega) = \left||F_{es}(j\omega)| - |\overline{F(j\omega)}|\right| \quad (23)$$

Referring to these definitions, we can find that through the compensation, the overall measurement deviation d_{sp} was reduced from 6.63 µm to 0.66 µm, i.e. by 90%, and the overall harmonic deviation D_h was reduced from 0.64 µm to 0.06 µm, thus also by 90%.

4. Harmonic hybridization to minimize the stochastic uncertainty

4.1 The algorithm of the hybrid F3S method

After compensating for the height difference of the probes, the measurement deviation can be greatly reduced. However, the probe outputs are still inevitably influenced by stochastic errors.

These random deviations can propagate to the measurement result. Shi [24] pointed out that in roundness measurements, when the determinant of transfer matrix $|W(\omega)|$ equals zero, the harmonic is suppressed and infinite harmonic deviation may occur in the result. When $|W(\omega)|$ is close to zero, the harmonic is sensitive to noise and a small stochastic disturbance can cause a large harmonic deviation. Analogously, the F3S straightness measurements may suffer from notable stochastic errors due to the suppressed and sensitive harmonics. Hence, to reduce the stochastic errors, and thus, to enhance the measurement precision, a hybrid F3S method is conceived here, which requires 4 steps as follows:

Step 1. Perform several F3S measurements.

Performing n candidate F3S measurements by choosing n different d, and n groups of Fourier coefficients of the workpiece profile are assessed. The the ω^{th} Fourier coefficient of the i^{th} group is expressed as $F(j\omega)_i$.

Step 2. Calculate the $|W(\omega)|$.

For Eq. (5), we obtain the transfer function from $F(j\omega)$ to $M(j\omega)$:

$$T(j\omega) = 1 - e^{j\frac{2\pi d}{L}\omega} \tag{24}$$

Then, the transfer matrix $W(\omega)$ can be computed via the Euler formula:

$$W(\omega) = \begin{pmatrix} 1 - cos\frac{2\pi d}{L}\omega & -sin\frac{2\pi d}{L}\omega \\ sin\frac{2\pi d}{L}\omega & 1 - cos\frac{2\pi d}{L}\omega \end{pmatrix} \tag{25}$$

Thus, the determinant of transfer matrix $|W(\omega)|$ can be computed:

$$|W(\omega)| = \begin{vmatrix} 1 - cos\frac{2\pi d}{L}\omega & -sin\frac{2\pi d}{L}\omega \\ sin\frac{2\pi d}{L}\omega & 1 - cos\frac{2\pi d}{L}\omega \end{vmatrix} \tag{26}$$

Eq. (26) shows that the d determines the $|W(\omega)|$, namely, determines the sensitivity of the individual harmonics to the noise.

When performing n candidate F3S measurements by choosing different d, n groups of $|W(\omega)|$ are achieved. The ω^{th} determinant of transfer matrix of the i^{th} F3S measurement is described as $|W(\omega)|_i$.

Step 3. Pick up the optimal Fourier coefficients.

For the same measurement section of the workpiece profile, the Fourier coefficients of the assessed harmonics are the same. However, when choosing different d, $|W(\omega)|$ is different. With this also the harmonics are influenced to varying degrees. Thus, there is a possibility to pick optimal Fourier coefficients from the n candidate assessments by the F3S method.

The Fourier coefficients $F(j\omega)_i$ are selected as the optimal ones corresponding to the largest determinant of the transfer matrix from the n candidate assessments by the F3S method:

$$F_{opt}(j\omega) = F(j\omega)_i \quad (i = \text{argmax}(|W(\omega)|_i)) \tag{27}$$

Here, argmax an operation that finds the argument i that gives the maximum value from $|W(\omega)|_i$.

Step 4. Compute the workpiece profile with the optimal Fourier coefficients.

Calculate the workpiece profile with the optimal Fourier coefficients $F_{opt}(j\omega)$ by applying the Inverse Fourier transform.

$$f(\theta) = F^{-1}\left[F_{opt}(j\omega)\right] \tag{28}$$

4.2 A simulation of the hybrid F3S method

A simulation of the hybrid F3S method was conducted to confirm its robustness to stochastic errors. To achieve this target, first, three F3S measurements were simulated, where d were 48.50 mm, 34.10 mm, and 78.60 mm, respectively. During the simulations, a stochastic signal noise of 2 µm RMS was added to the signals $m_1(\theta)$ and $m_{r2}(\theta)$ to simulate the stochastic errors. Thus, three sets of Fourier coefficients were estimated.

Then, by substituting the three values of d into Eq. (26), three sets of $|W(\omega)|$ were obtained (see Fig. 8). We can find that some $|W(\omega)|$ at a few harmonics are significantly smaller than that at other harmonics of the same F3S measurement, for instance, the 2^{nd}, 4^{th} and 29^{th} orders when d = 48.50 mm, the 3^{rd}, 6^{th}, and 9^{th} orders under d = 34.10 mm, and the 5^{th}, 9^{th} 14^{th}, and 28^{th} orders under d = 78.60 mm. We can conclude that these harmonics are sensitive and will imply significant harmonic uncertainties.

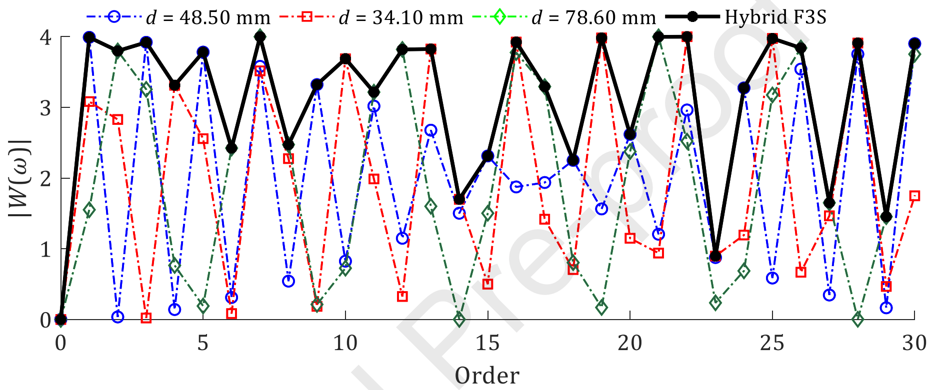

Fig. 8. The determinant of transfer matrix $|W(\omega)|$.

Third, according to $|W(\omega)|$, the optimal Fourier coefficients were selected from the three sets of measurement. From Fig. 8, we can find that $|W(\omega)|$ in the hybrid method as indicated by the black point always have the largest value. This suggests that the sensitive harmonics can be successfully avoided.

The estimated workpiece profiles were plotted in Fig. 9(a) and the harmonic deviations were also displayed in Fig. 9(b). From Fig. 9(b), we can find that some sensitive harmonics, which lead to large deviations, exist in the conventional F3S method, for instance, the 2^{nd} and the 4^{th} orders when d = 48.50 mm, the 3^{rd} and the 6^{th} orders when d = 34.10 mm, and the 14^{th} and the 28^{th} orders when d = 78.60 mm. These harmonics were included in the ones of the smaller $|W(\omega)|$ shown in Fig. 8. After employing the hybrid method, the sensitive harmonics have all been eliminated and the measurement deviations reduced significantly. Quantitatively, the overall measurement deviation d_{sp} was reduced by up to 8.5 μm (91%); the overall harmonic deviation D_h was reduced by 0.71 μm (89%).

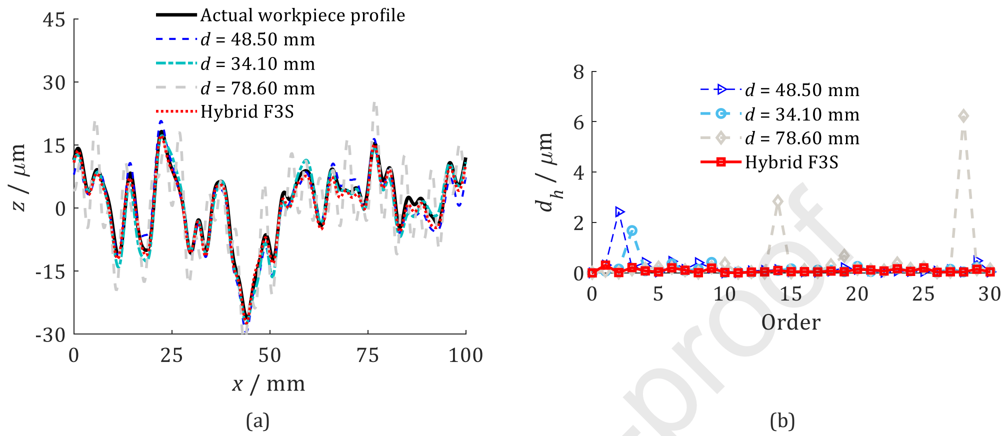

Fig. 9. Results of the hybrid F3S method and the conventional F3S method (a) the estimated profiles, and (b) the harmonic deviations.

Table 1

The overall deviation d_{sp} and D_h before and after utilizing the hybrid method.

Overall deviation	d / mm	F3S	Hybrid F3S
	48.50	0.8495	
d_{sp} / μm	34.10	1.2708	0.8204
	78.60	9.2918	
	48.50	0.1145	
D_h / μm	34.10	0.1953	0.0884
	78.60	0.7984	

5. Experimental setup

To verify the applicability in practice of the F3S and the hybrid F3S methods developed above, a graphite workpiece with a length of 150 mm was first machined on a grinding machine of

Takashima Multi Pro Ⅳ, and then, measured on the same machine. Three capacitive displacement probes, as indicated by P_1, P_2, and P_3 in Fig. 10, were mounted on the slide table by a specially designed fixture to detect the distance variation. The fixture has five mounting holes respectively at the positions of 0 mm, 34.10 mm, 48.50 mm, 78.60 mm, and 100 mm. The second and the third probes are always installed at the positions of 0 mm and 100 mm, respectively, while the first probe could be arbitrarily installed at the rest positions. This means that the measurement length L always equals 100 mm, while the measurement distance d can be varied depending on the mounting position of P_1.

During measurements, the feed rate v was kept constant at 5 mm/s along the X-axis. A NI 9125 digitizer was adopted to collect the distance signals with a sampling frequency of 1000 Hz. To investigate the repeatability of the measurement, 100 repeated measurements were performed under each condition.

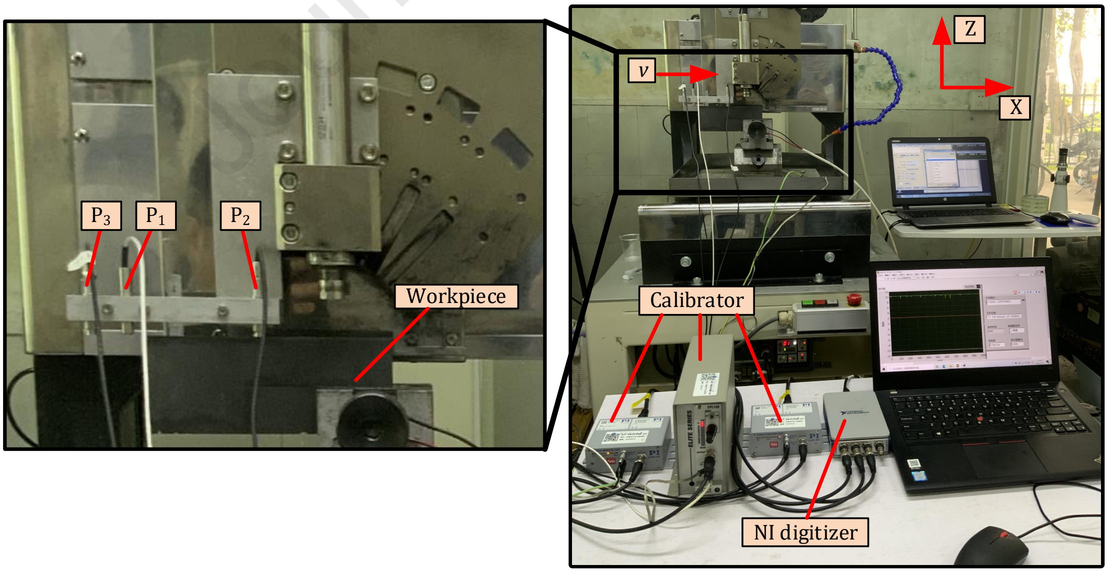

Fig. 10. Physical pictures of the experimental setup.

To verify the accuracy of the on-machine measurement, the workpiece profile was also measured off-line on a surface profilometry (Taylor surf CLI 1000, AMETEK, Inc., USA), as displayed in Fig. 11. In this instrument, inductive gauging was adopted, which possesses a measurement range of 2.5 mm and a resolution of 40 nm. Also, the slide straightness of the scanning axis is stated to be ±1 μm. The scanning speed v_1 was 500 μm/s and the sampling frequency was 1000 Hz, giving a sampling distance of 0.5 μm.

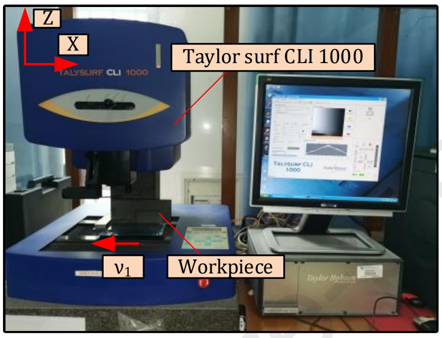

Fig. 11. The physical picture of the off-line measurement.

6. Results

6.1 Experiment of compensation of the probe height difference

Fig. 12 shows the signals before and after the compensation of the probe height difference. Distinctly, before the compensation, a step of 33.7 μm occurred at the joint point of 65.90 mm in the joint signal m_{r2} (in this example, d = 34.10 mm), as highlighted by yellow bars. The step has been completely removed after the compensation.

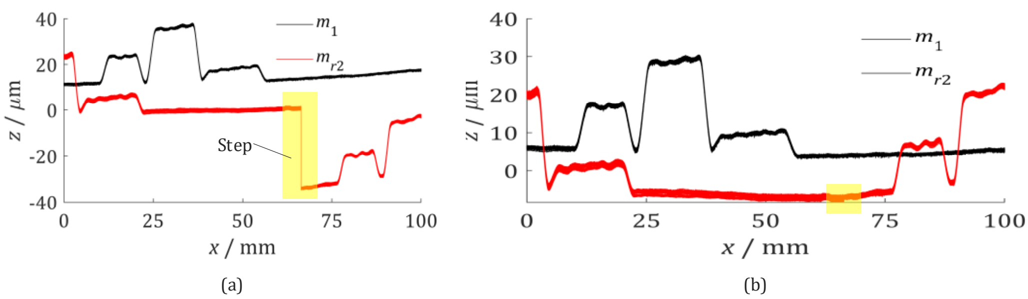

Fig. 12. The experimental signals of the probes, before (a) and after (b) the compensation.

The estimated profiles were plotted in Fig. 13. The profile obtained in the off-line measurement was also exhibited as a reference. It can be observed that in the spatial domain, the maximal measurement deviation has been reduced from 27 μm to 10 μm by the compensation.

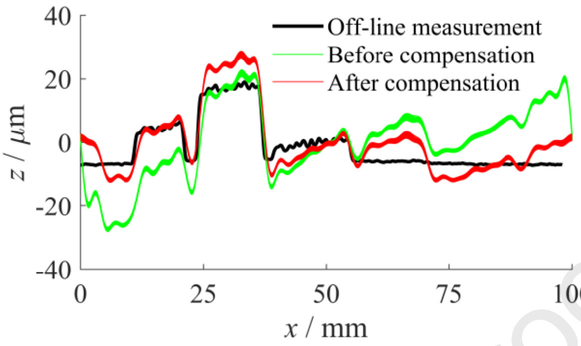

Fig. 13 Comparison of the workpiece profiles estimated by the F3S method before and after the compensation of the probe height difference.

To quantify the overall deviation, the 100 measured profiles were averaged and substituted into Eqs. (21) and (22). It was found that after the compensation, the overall measurement deviation d_{sp} was reduced from 9.2 μm to 3.9 μm (58%); the overall harmonic deviation D_h was reduced from 1.1 μm to 0.5 μm (55%), suggesting the effectiveness of the developed algorithm to compensate for the height difference.

6.2 Experiments of the hybrid F3S method

Fig. 14 shows the results of the F3S measurements when d = 48.50 mm, 34.10 mm, and 78.60 mm. From Fig. 14 (a), certain degrees of fluctuated deviations, which is up to 10 μm, can be observed. From the harmonic domain in Fig. 14 (b), we can clearly find that most of the harmonics estimated by the F3S measurements agreed well with that obtained in the off-line measurement, except for a few harmonics, such as (1) 2^{nd} order when d = 48.50 mm; (2) 3^{rd}, 6^{th} , and 12^{th} orders when d = 34.10 mm; and (3) 5^{th} and 19^{th} orders when d = 78.60 mm, as highlighted by blue bars. This suggests that the measurement deviation of the F3S measurements mainly arises from quite a few harmonics, which might be susceptible to error sources. For example, when $d =$ 78.60 mm, the measurement error mainly comes from the 5^{th} and the 19^{th} order harmonics.

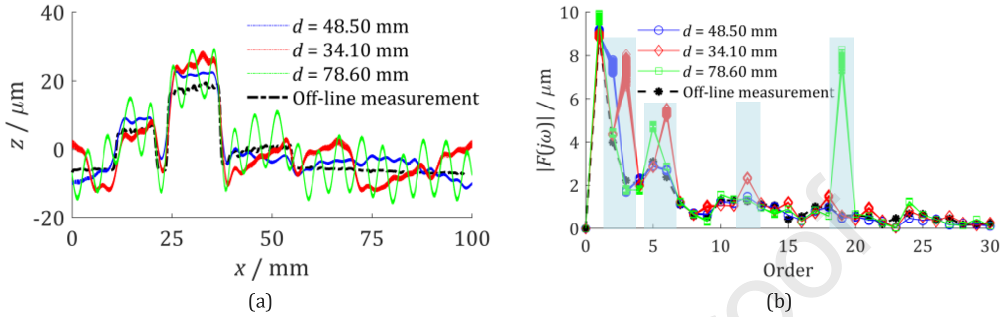

Fig. 14 Results of the F3S measurements: (a) the estimated profiles and (b) their spectrum.

The determinant of transfer matrix $|W(\omega)|$ was also computed and plotted in Fig. 15. We can find that the $|W(\omega)|$ at a few harmonics were significantly closer to zero than that at other harmonics, for instance: (1) the 2^{nd}, 4^{th}, and 29^{th} orders when $d = 48.50$ mm, (2) the 3^{rd}, 6^{th}, 9^{th}, 12^{th}, 15^{th}, and 18^{th} orders when $d = 34.10$ mm, (3) the 5^{th}, 14^{th}, 19^{th} and 24^{th} orders when $d =$ 78.60 mm. This shows that the sensitive harmonics could be quite well detected by $|W(\omega)|$. The most robust/optimal Fourier coefficients could be picked out individually from the three sets of the Fourier coefficient estimates according to $|W(\omega)|$. The selected optimal Fourier coefficients are also called the hybrid Fourier coefficients.

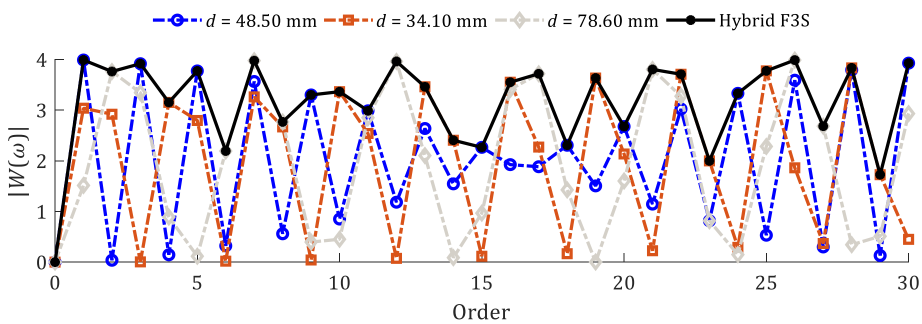

Fig. 15. The determinant of transfer matrix $|W(\omega)|$.

Finally, the straightness profile was computed from the hybrid Fourier coefficients of average value and shown in Fig. 16. We can find that the result matches quite well with the off-line measurement result in both the spatial and harmonic domain.

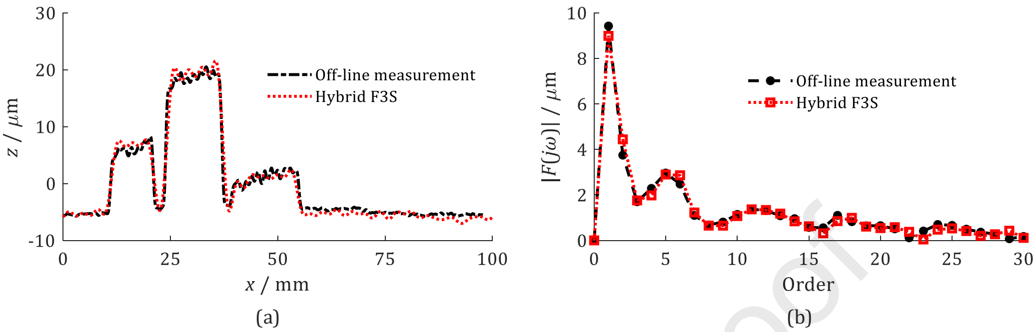

Fig. 16. Result of the hybrid F3S measurement: (a) the estimated profile and (b) the spectrum.

Fig. 17 shows the harmonic deviations obtained in the hybrid measurement and the conventional F3S measurements. We can find that when the hybrid method was adopted, minimal deviations could be achieved for almost all the harmonics. Moreover, the sensitive harmonics, which cause significant deviations, could be completely eliminated. This suggests that hybridization of the harmonic estimate could significantly enhance the robustness of the straightness profile measurement.

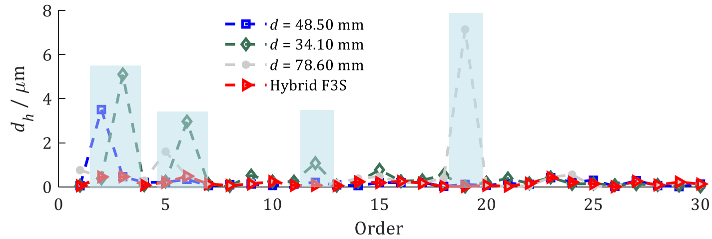

Fig. 17. The harmonic deviations of the hybrid F3S method and the F3S method.

After applying the hybrid F3S method, the measurement deviation was significantly reduced. Even compared with the optimal F3S method, the measurement deviation d_{sp} reduced from 2.5 μm to 1.1 μm (56%), and the overall harmonic deviation D_h was reduced from 0.27 μm to 0.17 μm

(37%), as shown in Table. 2.

Table 2

The overall deviation d_{sp} and D_h of experimental measurements.

overall deviation	d / mm	F3S	Hybrid F3S
d_{sp} / μm	48.50	2.5	1.1
	34.10	3.9	
	78.60	4.8	
D_h / μm	48.50	0.27	0.17
	34.10	0.50	
	78.60	0.52	

In this paper, a criterion U_{sp} is defined to estimate the repeatability of the measurement results, i.e. the random uncertainty:

$$U_{sp} = \sqrt{\frac{1}{MN_s}\sum_{k=1}^{N_s}\sum_{m=1}^{M}(f_m(k) - f_{mean}(k))^2} \quad (29)$$

Here, $f_{mean}(k)$ denotes the mean profile curve, given by $f_{mean}(k) = \frac{1}{M}\sum_{m=1}^{M} f_{\mathrm{m}}(k)$; $f_m(k)$ denotes the profile estimated in M repeated measurement; M equals 100.

Referring to Eq. (29), the random uncertainty in the conventional F3S measurements was calculated: 0.13 μm when $d = 48.50$ mm, 0.28 μm when $d = 34.10$ mm, and 0.21 μm when $d = 78.60$ mm, respectively. Also, the random uncertainty after adopting the hybrid method was computed to be 0.09 μm. This suggests that compared with the conventional F3S method, the hybrid F3S method can effectively reduce the random uncertainty greatly, or in other words, improve the reproducibility of the measurement results.

7. Conclusion

(1) The adverse effect of the height difference between the second and the third probes on the F3S measurement is clarified; subsequently, a numerical approach to estimate, as well as to

compensate for the height difference is proposed; the availability of the proposed method is numerically and experimentally verified.

(2) To alleviate the stochastic uncertainty, a hybrid F3S method is proposed: first, several sets of the Fourier coefficients of the straightness profile are obtained by performing the F3S measurements several times under different probe spacing; then, the optimal Fourier coefficients are picked out individually from the candidate estimates according to the determinant of the transfer matrix. The robustness of the hybrid F3S method to stochastic errors is confirmed numerically and experimentally.

(3) Practical straightness profile measurements were performed, respectively, on a grinding machine by adopting the hybrid F3S method and on a Taylor Hobson surface profiler. The results show that compared with the conventional F3S method, the hybrid F3S method reduced the measurement uncertainty considerably, and the straightness profile estimated by the hybrid method agreed well with the result off-line measured on the surface profiler.

Acknowledgments

This research is supported by the National Key Research and Development Program of China (Grant no. 2018YFB1701202), the National Natural Science Foundation of China (Grant nos. 52175507, 52111530095, 51975219, and 51805174), the Natural Science Foundation of Guangdong Province (Grant nos. 2021A1515011687 and 2020A1515010807), the Science and Technology Program of Guangzhou (No. 202102020755), and the Guangdong Science and technology Project (Grant No. 2020A0505100003), which are highly appreciated by the authors.

Reference

[1] Gao W, Huang P, Yamada T, Kiyono S. A compact and sensitive two-dimensional angle probe for

flatness measurement of large silicon wafers. Precision Engineering, 2002, 26(4): 396–404.

[2] Gao W, Kiyono S. Development of an optical probe for profile measurement of mirror surfaces. Optical engineering, 1997, 36(12): 3360-3366.

[3] Hwang J, Park C, Gao W, Kim S. A three-probe system for measuring the parallelism and straightness of a pair of rails for ultra-precision guideways. International Journal of Machine Tools & Manufacture, 2007, 47(7-8): 1053–1058

[4] Hwang J. Park C, Kim S. W. Estimation method for errors of an aerostatic planar XY stage based on measured profiles errors. The International Journal of Advanced Manufacturing Technology, 2010, 46: 877-883.

[5] ISO 230-7: 2006. Test Code for Machine Tools - Part 7: Geometric Accuracy of Axes of Rotation.

[6] Yang J. Present situation and prospect of error compensation technology for NC machine tools. Aeronautical Manufacturing Technology, 2012, 401(5): 40-45.

[7] Tong Z, Zhong W, Zeng W, Jiang X. Closed-loop form error measurement and compensation for FTS freeform machining. CIRP Annals - Manufacturing Technology. 70 (2021): 455-458

[8] Gao W, Haitjema H. Fang F. Leach R. Cheung C. Savio E. Linares J. On-machine and in-process surface metrology for precision manufacturing. CIRP Annals - Manufacturing Technology, 2019, 68(2): 843-866.

[9] Gao W, Tano M, Araki T, Kiyono S, Park C. Measurement and compensation of error motions of a diamond turning machine. Precision engineering, 2007, 31(3): 310-316.

[10] Whitehouse DJ. Some Theoretical Aspects of Error Separation Techniques in Surface Metrology. Journal of Physics E: Scientific Instruments, 1996, 9 (7):531-536.

[11] Tanaka H, Tozawa K, Sato H, O-hori M, Sekiguchi H. Taniguchi N. Application of new

straightness measurement method to large machine tool, CIRP Annals - Manufacturing Technology, 1981, 30(1): 455-459.

[12] Tozawa K, Sato H, O-hori M. A new method for the measurement of the straightness of machined tools and machined works. Journal of Mechanical Design, 1982, 104(3): 587-592.

[13] Wiegmann A, Schulz M, Elster C. Absolute profile measurement of large moderately flat optical surfaces with high dynamic range. Optics Express, 2008, 16(16): 11975-11986.

[14] Tanaka H, Sato H. Extensive Analysis and Development of Straightness Measurement by Sequential-Two-Points Method. Journal of Engineering for Industry, 1986, 108(3): 176-182.

[15] Gao W, Yokoyama J, Kojima H, Kiyono S. Precision measurement of cylinder straightness using a scanning multi-probe system. Precision Engineering, 2002. 26 (3): 279-288.

[16] Elster C, Weingärtner I, Schulz M. Coupled distance sensor systems for high-accuracy topography measurement: Accounting for scanning stage and systematic sensor errors. Precision Engineering, 2006, 30: 32–38.

[17] Kiyono S, Gao W. Profile measurement of machined surface with a new differential method. Precision Engineering, 1994, 16(3): 212-218.

[18] Gao W, Kiyono S. High accuracy profile measurement of a machined surface by the combined method. Measurement, 1996, 19(1): 55-64.

[19] Gao W, Kiyono S. On-Machine Profile Measurement of Machined Surface Using the Combined Three-Point Method. JSME International Journal Series C Mechanical Systems, Machine Elements and Manufacturing, 1997, 42(2): 253-259.

[20] Li C., Li S, Yu J. High-resolution error separation technique for in-situ straightness measurement of machine tools and workpieces. Mechatronics, 1996, 6(3): 337-347.

[21] Fung E, Yang S. An error separation technique for measuring straightness motion error of a linear slide. Measurement Science and Technology, 2000, 11: 1515-1521

[22] Fung E. A new method for measuring straightness and yawing motion errors of a linear slide. Journal of Manufacturing Science and Engineering, 2006, 128(2): 503-512.

[23] Fung E. An experimental five-sensor system for measuring straightness and yawing motion errors of a linear slide. Measurement Science and Technology, 2008, 19(7): 075102.

[24] Shi S, Lin J, Wang X, Zhao M. A hybrid three-probe method for measuring the roundness error and the spindle error. Precision Engineering, 2016, 45: 403–413.

[25] Shi S, Zhang H, Qu J, Jin G, Kuschmierz R, Czarske J. Measurement uncertainty propagation in spindle error separation techniques - Investigation by means of stochastic spectral method. International Journal of Machine Tools & Manufacture, 141(2 019): 36–45.

[26] Shi S, Kuschmierz R, Zhang G, Lin J, Czarske J, Qu J. Modeling, quantification, and mitigation of uncertainty propagation in two-step roundness measurements. Measurement, 2020, 155: 107530.

[27] Shi S, Haitjema H, Wang Y, Jin G. Uncertainty evaluation and reduction in three-probe roundness profile measurement based on the system transfer function, Precision Engineering, 2021, 68: 139-157.

Highlights:

1. Fourier 3-sensor method, resorting to Laplace transform, is proposed
2. Numerical solution to remove height difference between probes is proposed.
3. Hybrid Fourier 3-sensor method is proposed to improve measurement uncertainty.
4. Workpiece profile is measured by a Taylor surf CLI 1000 as a reference.

Declaration of interests

☒ The authors declare that they have no known competing financial interests or personal relationships that could have appeared to influence the work reported in this paper.

☐The authors declare the following financial interests/personal relationships which may be considered as potential competing interests: